



Experimental procedure to obtain 2D time-space high-speed water surfaces

Bateman, A. ; Granados, Albert; Medina, V. ; Velasco, D. ; Nalesso, M.

Published in:

Proceedings of the International Conference of Fluvial Hydraulics (2006)

Publication date:

2006

Document Version

Peer reviewed version

[Link back to DTU Orbit](#)

Citation (APA):

Bateman, A., Granados, A., Medina, V., Velasco, D., & Nalesso, M. (2006). Experimental procedure to obtain 2D time-space high-speed water surfaces. In *Proceedings of the International Conference of Fluvial Hydraulics (2006)* (pp. 1879-1888). CRC Press, Taylor & Francis Group.

General rights

Copyright and moral rights for the publications made accessible in the public portal are retained by the authors and/or other copyright owners and it is a condition of accessing publications that users recognise and abide by the legal requirements associated with these rights.

- Users may download and print one copy of any publication from the public portal for the purpose of private study or research.
- You may not further distribute the material or use it for any profit-making activity or commercial gain
- You may freely distribute the URL identifying the publication in the public portal

If you believe that this document breaches copyright please contact us providing details, and we will remove access to the work immediately and investigate your claim.

Experimental procedure to obtain 2D time-space high-speed water surfaces

A. Bateman

Hydraulic, Maritime and Environmental Engineering Department, GITS-UPC. Technical University of Catalonia, Spain. DI, c/Gran Capitan s/n, 08034, Barcelona, Spain. E-mail: allen.bateman@upc.edu

A. Granados

Hydraulic, Maritime and Environmental Engineering Department, GITS-UPC. Technical University of Catalonia, Spain. DI, c/Gran Capitan s/n, 08034, Barcelona, Spain. E-mail: Alberto.Granados@estudiant.upc.edu

V. Medina

Hydraulic, Maritime and Environmental Engineering Department, GITS-UPC. Technical University of Catalonia, Spain. DI, c/Gran Capitan s/n, 08034, Barcelona, Spain. E-mail: vicente.medina@gits.ws

D. Velasco

Hydraulic, Maritime and Environmental Engineering Department, GITS-UPC. Technical University of Catalonia, Spain. DI, c/Gran Capitan s/n, 08034, Barcelona, Spain. E-mail: david.velasco@upc.edu

M. Nalesso

Fluid Mechanics Institute. Central University of Venezuela. E-mail: mnalesso@imf.ing.ucv.ve

ABSTRACT: Numerical validations always require a major effort involving laboratory measurements. In 2D models, it is unusual to see comparisons between measurements (in space and time) and the numerical results of a model. Measuring a surface involves many problems because collecting sufficient data in space and time is very complex. This paper indicates how to measure a liquid surface by taking 2D measurements (in space and time) of a set of cross-sections of a water surface experiencing a dam-break phenomenon. This work was carried out by a research group (GITS-UPC) at the Hydraulics Laboratory of the Department of Hydraulic, Maritime and Environmental Engineering of the Technical University of Catalonia. The paper details our mathematical framework and experimental methodology, which involves 3 mW laser beams and high- and medium-speed cameras, and compares a numerical surface to an experimental surface. The numerical data were modelled using FLATMODEL, which was developed entirely by the research group.

1 INTRODUCTION

Mathematical sketching is a method that can deal with very complex problems. It is also very clear and introduces the new concept of making hydraulic laboratory measurements using images. This method can recreate 3D representations of high-speed flow surfaces in space and time, using a single photograph for each time step. Cameras have already been used in laboratories to recreate certain physical phenomena, but here an entire surface is recreated at each instant to calibrate a 2D model. Here we present the mathematical methodology used to scan surfaces and its application to a dam-break problem. We developed this technique for characterizing moving surfaces in order to calibrate a 2D Saint-Venant numerical code and evaluate the divergence of the model from reality.

2 POINTS, SPACE AND PLANE CORRESPONDENCE

Figure 1 shows that taking a picture is like projecting one point in space onto a point

photograph through a point called the focus (F). This projection is determined by fixing a reference point in space, knowing the position of the camera plane and locating the focus. That is, for each point in space, it is possible to determine the corresponding pixel of the photograph by noting where the straight line defined by the point and the focus intersects with the photograph plane. However, it is practically impossible and unnecessary to know all of these parameters directly. Through projective geometry, an application known as camera calibration can project the point from the reference in space to the coordinates in the photograph (real coordinates or pixels) without explicitly needing to know these parameters.

2.1 From space to the photograph: Direct Linear Transformation (DLT) (Abdel-Aziz, 1971 and Faugeras 1993)

¿How can the corresponding point in the photograph be obtained for a given point $x_e = (x_1 \ x_2 \ x_3)$ in space

in any reference R_e (Figure 1)? If we know the equation of the photograph plane $\Pi_f : ax + by + cz + d = 0$, and the coordinates of the focus $F = (F_1 \ F_2 \ F_3)$, then the point to be determined in the reference R_e is given by the intersection of the line $r : (x \ y \ z) = F + \lambda(F - x^e)$ with the plane Π_f (Figure 1). However, in addition to being nonlinear in the x_e coordinates, this equation depends on parameters that are impossible to define directly, i.e. the expression in the reference R_e for the photograph plane Π_f and the focus F . We need another way to find the projected point in the photograph.

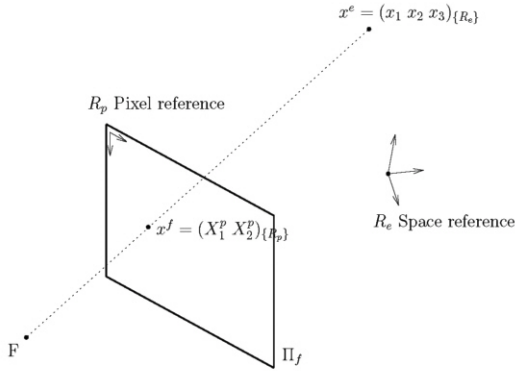


Figure 1. Space and photograph reference.

Imagine that, instead of taking a space R_e as a reference, we take a reference R_c (Figure 2), which we will call the camera reference. The axis z of this reference is perpendicular to the plane Π_f , with origin at the focus F . This reference is located at a distance of 1 from the photograph plane (focal distance). In these conditions, the straight line r has the mathematical expression

$r: (x \ y \ z)_{\{R_c\}} = \lambda(x_1 \ x_2 \ x_3)_{\{R_c\}}$ and the plane is $\Pi_f : z_{\{R_c\}} = 1$. Therefore, their intersection is

$x^j_{\{R_c\}} = \begin{pmatrix} x_1 & x_2 \\ x_3 & x_3 \end{pmatrix} 1$. Instead of projecting the point

$x^e(x_1 \ x_2 \ x_3)_{\{R_c\}}$, a multiple of it,

$\mu x^e = (\mu x_1 \ \mu x_2 \ \mu x_3)_{\{R_c\}}$, is projected, which is the

same as projecting x^e . This is because both points are in the same straight line, $r = \lambda(x_1 \ x_2 \ x_3)_{\{R_c\}}$, which is perpendicular to the projective plane Π_f .

Therefore, the intersection with the plane is the same for both points.

Rather than relating points in the space with points in the plane, the idea is to relate the lines in \mathbb{R}^3 that pass through the origin (F) to points of the plane Π_f . Thus, we can relate the direction of the straight line $r = \lambda(x_1 \ x_2 \ x_3)_{\{R_c\}}$, which is the point

$(x_1 \ x_2 \ x_3)_{\{R_c\}}$ and all of its multiples, with the point

$\begin{pmatrix} x_1 & x_2 \\ x_3 & x_3 \end{pmatrix} 1$ of the photograph plane.

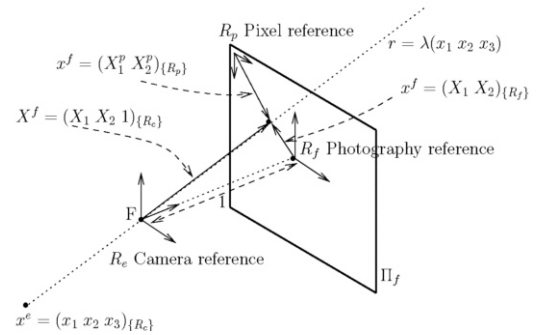


Figure 2. Camera reference.

We must also project straight lines that are parallel to the plane Π_f . To do so, we must construct an abstract mathematical object that defines points of infinity or improper points. This is the vectorial space known as projective plane \mathbb{P}_2 , which is the same as plane Π_f , except for the improper points that we cannot see but can manipulate algebraically. In \mathbb{P}_2 , we can use the following homogeneous coordinates: if $(x_1 \ x_2 \ x_3) \in \mathbb{R}^3$ with $x_3 \neq 0$, the straight line will be represented by the point $\begin{bmatrix} 1 & x_1 & 0 \\ x_2 & & \end{bmatrix}$. The improper points are then represented by points whose third component is equal to 0 in the homogeneous coordinates.

With the sole aim of grouping all the representative elements of \mathbb{P}_2 in one element, it is common to use the generalized coordinates. This consists in eliminating the third coordinate when it is 1 (that is, when the point is not improper). Then, the rest of the coordinates are represented as:

$(X_1 \ X_2) = \begin{pmatrix} x_1 & x_2 \\ x_3 & x_3 \end{pmatrix}$. Whenever we work with

improper points, which implies using a plane that is parallel to the photograph and passes through the focus F , it makes no sense. In such a case, we work with the region of \mathbb{P}_2 called D , which corresponds to the photograph paper and does not contain improper points.

We can identify the generalized coordinates $(X_1 \ X_2)_{\{R_f\}} \in \mathbb{P}_2$ as the point x_f in real coordinates in the photo reference. This reference is obtained by orthogonally projecting the axes $x - y$ of the camera reference over the plane Π_f (Figure 2). That is,

$x_f = (X_1 \ X_2)_{\{R_f\}} \in \mathbb{R}_2$.

Now we want to work with a reference R_p (pixel reference) other than R_f , with the origin in the upper-left corner of the photograph (see Figure 2), in which the points of the photograph are expressed in pixels. A new change of reference must therefore be added.

A change of reference in the plane can be written in matrix form as

$$\begin{pmatrix} X_1^p \\ X_2^p \\ 1 \end{pmatrix}_{\{R_p\}} = \begin{pmatrix} r_{11} & r_{12} & t_x \\ r_{21} & r_{22} & t_y \end{pmatrix} \begin{pmatrix} X_1 \\ X_2 \\ 1 \end{pmatrix}_{\{R_f\}} \quad (1)$$

in which the vector $(t_x \ t_y)$ represents the translation of the origin and the matrix $(r_{ij})_{ij}$ represents the basis change due to the rotation of the axis system. Before performing the transformation in \mathbb{R}_2 , it is a good idea to perform another change of reference in the projective plane. Thus, in homogeneous coordinates, the change takes the form of a linear application, Φ_2 , of \mathbb{P}_2 .

$$\begin{pmatrix} X_1^p \\ X_2^p \\ 1 \end{pmatrix}_{\{R_p\}} = \begin{pmatrix} r_{11} & r_{12} & t_x \\ r_{21} & r_{22} & t_y \\ 0 & 0 & 1 \end{pmatrix} \begin{pmatrix} X_1 \\ X_2 \\ 1 \end{pmatrix}_{\{R_f\}} \quad (2)$$

Hitherto we have seen how to relate points in space with those of the photograph if the former are expressed in some reference denoted by $\{R_c\}$ (camera reference). However, as detailed above, it is impossible to have the points in \mathbb{R}^3 in that reference because they depend on the position of the focus and the photograph plane, which cannot be determined directly.

If we have properly selected the points at reference $\{R_e\}$ (Figure 1), and we assume that there exists an application that passes the points from $\{R_e\}$ to $\{R_c\}$, this is a change of reference in \mathbb{R}^3 similar to (1) but in \mathbb{R}^3 instead of \mathbb{R}^2 .

$$\begin{pmatrix} x_1^c \\ x_2^c \\ x_3^c \\ 1 \end{pmatrix}_{\{R_c\}} = \begin{pmatrix} r_{11} & r_{12} & r_{13} & t_x \\ r_{21} & r_{22} & r_{23} & t_y \\ r_{31} & r_{32} & r_{33} & t_z \end{pmatrix} \begin{pmatrix} x_1 \\ x_2 \\ x_3 \\ 1 \end{pmatrix}_{\{R_e\}} \quad (3)$$

Like (2), it can change the reference in \mathbb{R}^3 into a linear application from \mathbb{P}_3 to \mathbb{P}_3 .

$$\begin{pmatrix} x_1^c \\ x_2^c \\ x_3^c \\ 1 \end{pmatrix}_{\{R_c\}} = \begin{pmatrix} r_{11} & r_{12} & r_{13} & t_x \\ r_{21} & r_{22} & r_{23} & t_y \\ r_{31} & r_{32} & r_{33} & t_z \\ 0 & 0 & 0 & 1 \end{pmatrix} \begin{pmatrix} x_1 \\ x_2 \\ x_3 \\ 1 \end{pmatrix}_{\{R_e\}} \quad (4)$$

By calling this linear application Φ_1 , we can define a linear application A from \mathbb{P}_3 to \mathbb{P}_2 .

The composition $\Phi_1 \circ A \circ \Phi_2$ as a linear application M between \mathbb{P}_3 and \mathbb{P}_2 includes the changes of reference and the projection in a strict sense. Therefore, this method is called Direct Linear Transformation (DLT).

The linear transformation can be written as

$$\begin{bmatrix} n.X_1^p \\ n.X_2^p \\ n \end{bmatrix} = \begin{pmatrix} m_{11} & m_{12} & m_{13} & m_{14} \\ m_{21} & m_{22} & m_{23} & m_{24} \\ m_{31} & m_{32} & m_{33} & m_{34} \end{pmatrix} \begin{bmatrix} x_1^e \\ x_2^e \\ x_3^e \\ 1 \end{bmatrix} \quad (5)$$

in which $M = (m_{ij})_{ij}$.

Why does n appear here? It was omitted in the previous reasoning. In fact, a change of reference in \mathbb{R}^2 is assumed to be a basis change in \mathbb{P}_2 in homogeneous coordinates. However, changes of this sort are determined by just three points in \mathbb{R}^3 , except for proportionality factors. The 3×3 basis-change matrix Φ_2 gives three points of \mathbb{R}^3 to determine a basis change in homogeneous coordinates in \mathbb{P}_2 . However, four points are needed to determine the transformation uniquely. The same occurs in a change of reference in \mathbb{R}^3 . Five points of \mathbb{R}^4 are needed to uniquely determine a basis change in \mathbb{P}_3 , but only four points are given: the three vectors of the coordinates and the origin. Then, n represents the two proportionality factors of the basis change that are omitted.

Therefore, a projection of a point from \mathbb{R}^3 over a plane Π_f is determined by a linear application M of \mathbb{P}_3 in \mathbb{P}_2 , except for a proportionality factor n . That is, the third coordinate of a point in \mathbb{P}_2 obtained by applying M is not equal to 1. To obtain $(X_1^p \ X_2^p)$, the first two coordinates of the obtained point are divided by the third component when changing from \mathbb{P}_2 to \mathbb{R}^2 .

Finally, the matrix M can be obtained numerically by relating known points in space with points in the

photograph. This process is known as camera calibration.

2.2 From the photograph to space: the inverse process (Hatze, 1988) or (Chen, 1994)

Once we have obtained the projectivity that connects the points in space with the points in the photograph through the focus, we can use the inverse process to obtain the point we need. However, a given point in the photograph plane is not represented by a single point in space but by a whole line projected through it. We need more information about the position of the point to be determined in space – for example, a plane that it belongs to.

Algebraically, the matrix M is not square, and it makes no sense to evaluate the inverse, at least not without limiting the starting space \mathbb{P}_3 to the homogenized points of \mathbb{R}^3 located in a certain plane. Then, the dimension of the arriving and starting space equals converting the projectivity in an isomorphism between the projective spaces.

From a practical point of view, it is a good idea to request that the points to be surveyed belong to a certain known plane.

Imagine that we know the projection matrix transformation M and that the point to be determined in \mathbb{R}^3 , $(x_1 \ x_2 \ x_3)$, belongs to a known plane defined by the equation $\Pi : ax_1 + bx_2 + cx_3 + d = 0$. In homogeneous coordinates, the point x^f can be written as $x^f = [X_1 \ X_2 \ 1]$ and the plane can be written as

$$\Pi : ax_1 + bx_2 + cx_3 + dx_4 = 0 \quad (6)$$

The point to be determined is $x^e = [x_1 \ x_2 \ x_3 \ x_4] \in \mathbb{P}^3$ anti-image by M of x^f (in homogeneous coordinates) that fits equation (6). Using points x^f and x^e , the following equation is obtained from (5):

$$\begin{cases} 1 = m_{31}x_1 + m_{32}x_2 + m_{33}x_3 + m_{34}x_4 \\ X_1 = m_{11}x_1 + m_{12}x_2 + m_{13}x_3 + m_{14}x_4 \\ X_2 = m_{21}x_1 + m_{22}x_2 + m_{23}x_3 + m_{24}x_4 \end{cases} \quad (7)$$

In some way, x_4 plays the role of n in equation (5). If $a \neq 0$, we can write:

$$x_1 = -\frac{bx_2 + cx_3 + dx_4}{a} \quad (8)$$

By substituting the value of (8) in (7), the following system is obtained in matrix notation:

$$\begin{bmatrix} X_1 \\ X_2 \\ 1 \end{bmatrix} = \begin{bmatrix} \left(m_{12} - \frac{m_{11}b}{a}\right) + \left(m_{13} - \frac{m_{11}c}{a}\right) + \left(m_{14} - \frac{m_{11}d}{a}\right) \\ \left(m_{22} - \frac{m_{21}b}{a}\right) + \left(m_{23} - \frac{m_{21}c}{a}\right) + \left(m_{24} - \frac{m_{21}d}{a}\right) \\ \left(m_{32} - \frac{m_{31}b}{a}\right) + \left(m_{33} - \frac{m_{31}c}{a}\right) + \left(m_{34} - \frac{m_{31}d}{a}\right) \end{bmatrix} \begin{bmatrix} x_2 \\ x_3 \\ x_4 \end{bmatrix} \quad (9)$$

in which the matrix of (9) is the restriction for Π of M , which is square, and it is possible to find the points x_2, x_3 and x_4 (x_1 is defined by the known plane Π through (8)). To obtain the point x^e , the homogeneous coordinates $(x_1 \ x_2 \ x_3 \ x_4)$ are divided by x_4 to obtain 1 in the last element or coordinate. That is, it is de-homogenized:

$$(x_1^e \ x_2^e \ x_3^e) = \frac{\begin{pmatrix} -\frac{bx_2 + cx_3 + dx_4}{a} \ x_2 \ x_3 \end{pmatrix}}{x_4} \quad (10)$$

To sum up, given a point in the photograph $x^f = [X_1 \ X_2] \in \mathbb{R}^2$, it is homogenized to obtain $x^f = [X_1 \ X_2 \ 1] \in \mathbb{P}^2$.

Then, $x^e = [x_1 \ x_2 \ x_3 \ x_4] \in \mathbb{P}^3$ is calculated using equations (8) and (9). Finally, it is de-homogenized to obtain $x^e = (x_1^e \ x_2^e \ x_3^e) = \left(\frac{x_1}{x_4} \ \frac{x_2}{x_4} \ \frac{x_3}{x_4}\right) \in \mathbb{R}^3$.

2.3 Determining the matrix M or projectivity: Camera calibration

In the system of equations (5), the unknowns are the parameters of the M matrix m_{ij} . For each point in space $(x_1 \ x_2 \ x_3)$ and its correspondents in the photograph $(X_1 \ X_2)$, two equations (solved for n) can be obtained as follows:

$$\begin{aligned} m_{31}x_1X_1 + m_{32}x_2X_1 + m_{33}x_3X_1 + m_{34}X_1 \\ - m_{11}x_1 - m_{12}x_2 - m_{13}x_3 - m_{14} = 0 \\ m_{31}x_1X_2 + m_{32}x_2X_2 + m_{33}x_3X_2 + m_{34}X_2 \\ - m_{21}x_1 - m_{22}x_2 - m_{23}x_3 - m_{24} = 0 \end{aligned} \quad (11)$$

At first glance, then, it seems that we will need the correspondence of at least six points in space and six points in the photograph, since there are twelve unknowns and each pair of points gives two equations.

Nevertheless, the system defined by (11) is homogeneous, and a trivial solution $m_{ij} = 0$ always exists. In fact, the value of n is undetermined because it has a value of zero, which makes no sense.

If this parameter n does not exist, we can determine the values of m_{ij} simply by giving four points. However, this is not the case. In order to solve the problem, we must therefore add a restriction to the matrix M .

Suppose we have the points in space expressed in the camera reference used above (Figure 2). In these circumstances, the matrix projection M has the following form (Faugeras, 1993), (Olagué, 2001):

$$M_c = \begin{pmatrix} -f & 0 & u_0 & 0 \\ 0 & -f & v_0 & 0 \\ 0 & 0 & 1 & 0 \end{pmatrix} \quad (12)$$

where $(u_0 \ v_0)$ are the coordinates of the centre of the photograph (focus projection) in the pixel system and f is the focal (Chen, 1994). This matrix corresponds to $M_c = \Phi_2$. To work in the reference \mathbb{R}^3 , $\{R_e\}$, M can be composed with the basis change Φ_1 , that is:

$$M = M_c \cdot \Phi_1 \quad (13)$$

in which

$$\Phi_1 = \begin{pmatrix} r_{11} & r_{12} & r_{13} & t_x \\ r_{21} & r_{22} & r_{23} & t_y \\ r_{31} & r_{32} & r_{33} & t_z \\ 0 & 0 & 0 & 1 \end{pmatrix} = \begin{pmatrix} r_1 & t_x \\ r_2 & t_y \\ r_3 & t_z \\ 0 & 1 \end{pmatrix} \quad (14)$$

is the basis change in \mathbb{P}_3 in Equation (4).

This decomposition makes it possible to find a projection matrix M through the intrinsic parameters (M_c) and extrinsic parameters (Φ_1) of the camera.

The submatrix $\Phi_1(r_i)_{(i)}$, in which r_i is a row vector of a composition of rotations, requires that $\|r_3\| = 1$ (Pizarro, 2005). From (13), it follows that

$$\sqrt{m_{31}^2 + m_{32}^2 + m_{33}^2} = 1 \quad (15)$$

With this restriction, there are now eleven unknowns instead of twelve. The new unknown matrix can be written as: (Chen, 1994)

$$L = \begin{pmatrix} m_{11} & m_{12} & m_{13} & m_{14} \\ m_{34} & m_{34} & m_{34} & m_{34} \\ m_{21} & m_{22} & m_{23} & m_{24} \\ m_{34} & m_{34} & m_{34} & m_{34} \\ m_{31} & m_{32} & m_{33} & 1 \\ m_{34} & m_{34} & m_{34} & \end{pmatrix} = \begin{pmatrix} L_1 & L_2 & L_3 & L_4 \\ L_5 & L_6 & L_7 & L_8 \\ L_9 & L_{10} & L_{11} & 1 \end{pmatrix} \quad (16)$$

By pairing n points in space $(x_i \ y_i \ z_i)_i$ with n points in the photograph $(X_i \ Y_i)_i$ and applying the change of variables to (11), the new system to be solved is made up of a system with eleven unknowns and $2n$ equations, as:

$$\begin{pmatrix} x_i & y_i & z_i & 1 & 0 & 0 & 0 & 0 & -x_i \cdot X_i & -y_i \cdot X_i & -z_i \cdot X_i \\ 0 & 0 & 0 & 0 & x_i & y_i & z_i & 1 & -x_i \cdot Y_i & -y_i \cdot Y_i & -z_i \cdot Y_i \\ & & & & & & & & \vdots & & \end{pmatrix} \cdot \begin{pmatrix} L_1 & L_2 & \dots & L_{10} & L_{11} \end{pmatrix}^T = \begin{pmatrix} X_i & Y_i & \dots \end{pmatrix}^T \quad (17)$$

This system is over-determined and can be solved using the least-squares method.

Once the system has been solved, to recover the projective matrix M , it follows that:

$$M = \frac{1}{\sqrt{L_9^2 + L_{10}^2 + L_{11}^2}} \begin{pmatrix} L_1 & \dots & \dots & L_4 \\ \vdots & \ddots & \ddots & \vdots \\ L_9 & \dots & \dots & L_{12} \end{pmatrix} \quad (18)$$

thereby undoing the change of variables and imposing the restriction (15).

3 EXPERIMENTAL SET-UP

3.1 Flume dam break

We studied the changes over time in water-surface position (height) caused by suddenly opening the gate. The experiment involved high-speed movements in the water surface, which were recorded with two different digital cameras: a high-speed Basler camera and a medium-speed Lumenera camera.

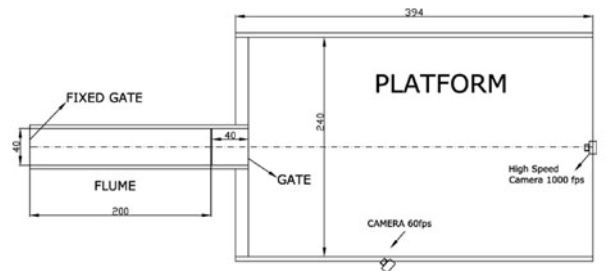


Figure 3. Flume and platform set-up and the positions of cameras, with dimensions in cm.

The first experiment was a typical one. A flume filled with water was controlled by a sluice gate and connected directly to a platform, as shown in Figure 3. The platform was initially dry. The gate was removed manually from its original position and water flowed from the flume to the platform. The flume used in the first experiment was 9 m long, 40 cm wide and 60 cm high. It was tilted from 0 to 27°.

The flume ended at a platform 4 m long, 2.4 m wide and 60 cm tall. In this experiment, the effective flume length was just 2 m (Figure 3). A fixed volume of water was held between two gates about 2 m apart. This part of the flume was connected to the platform by a manual sluice gate. A 50 cm deep volume of water was held.

Between 5 and 10 parallel laser beams were placed vertically over the platform, generating lines perpendicular to the flume axis in order to obtain cross-sections of the water surface. The water was mixed with milk at a concentration of 2% so that it would reflect the laser beams and make it possible to take photographs. Higher concentrations of milk caused more reflection, and lower concentrations allowed the light to penetrate the mixing fluid to a greater degree. We tried out different mixtures and found that the minimum concentration of milk was about 2% by volume. This allowed us to use as little milk as possible and obtain strips of light that were not too thick, thus preventing them from overlapping.

The Basler camera can capture images at up to 1000 fps with a resolution of 1200x1000 pixels or more, depending on the frame size. The Basler camera used normal Nikon lenses that produce high-quality images without optical aberration. The Lumenera camera had higher luminescence than the Basler because its lens had higher luminescence and also because the Basler's minimum shooting frequency was higher. The Lumenera had a wide-angle lens, which caused significant image deformation, which had to be corrected. A new MATLAB code was produced to correct this aberration.

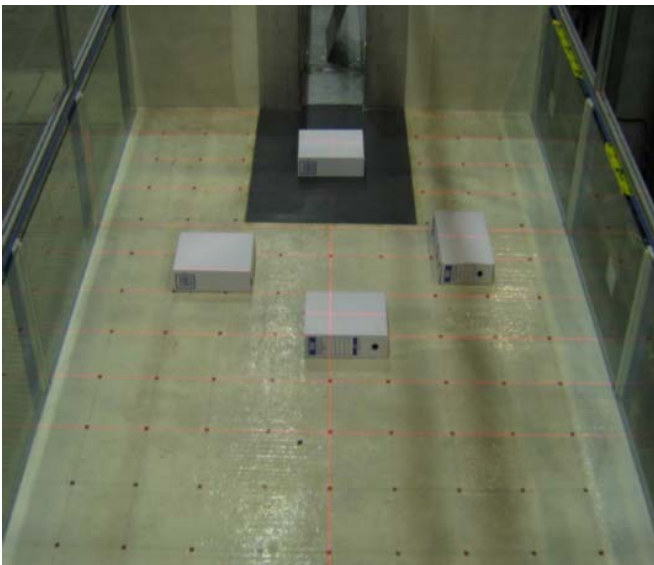


Figure 4. Lasers and general view of the experimental set-up.

A series of photographs of the light reflecting from the mixture were taken and processed. The idea was to obtain different cross-sections of the surface using the laser beams, in order to reconstruct the surface at each time step. We could not use many lasers because the beams could have overlapped and the

numerical process would have failed. A minimum distance was therefore maintained between lasers.

3.2 Camera position

The cameras were placed in such a way that the projection of the laser beams in the film did not cross at any time. They needed to be able to perceive water-level fluctuations accurately. In our experiments, the camera angle ranged from 20 to 30°. The camera distance depended on the area being analysed. Neither the distance nor the angle mattered because the camera needed to be calibrated and there were intrinsic values throughout the process.

3.3 Camera calibration

Once the aberration had been corrected, the camera needed to be calibrated. As mentioned above, at least six points must be identified in the space of known coordinates and correlated with six points in the photograph in order to determine the M projection matrix. As a calibration object, we used a meshed box located in a known position (**¡Error! No se encuentra el origen de la referencia.5**).

The points in the space used to calibrate the camera were located throughout the volume of study in order to avoid extrapolation problems that would increase the estimation error. We used a set of points taken from different positions of the meshed object in the area of interest.

3.4 Detection of laser beams

There are various techniques for finding the pixels that belong to a laser beam in a photo. Depending on the quality of the photograph, the layout of the laser beams, the contrast of the beams, the background of the image and other factors, one technique may be better than another. All techniques require a pre-filtering or post-filtering process. Here we present two different techniques, detection by maximum and morphological image treatment, which we applied to two cameras that observed the same experiment from different positions. Frontal (Basler) and lateral (Lumenera) points of view were used in the subsequent analysis, as shown in **¡Error! No se encuentra el origen de la referencia.6**.

The frontal view had certain advantages over the lateral view. The main advantage lies in the layout of the laser beams in the photograph. It was easy to apply an intuitive technique to detect the maximum of the column of pixels (by colour index), which match up with the laser beams.

The photograph resolution of the Basler camera was higher than that of the Lumenera camera. The area of study occupied the entire frame area and we were able to obtain more information about the process. However, in this specific example, the

frontal view presented a difficulty: the image could not describe the high lateral gradients of the flow as well as images from the lateral view did. See Figure 6 to appreciate this problem.

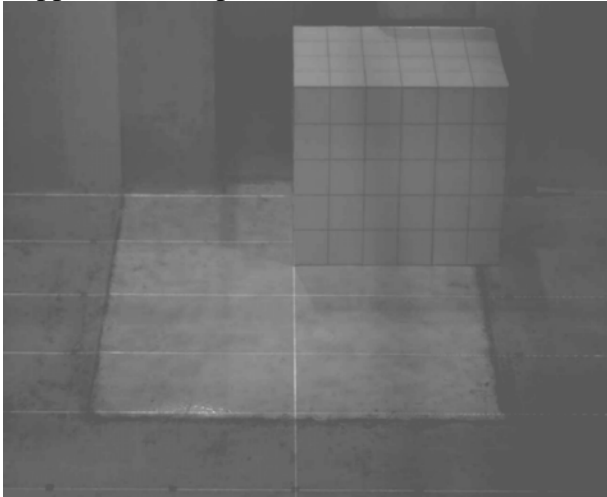


Figure 5. Meshed box used in the calibration procedure.

3.5 Laser-beam detection techniques. Frontal view.

First, we corrected the photograph by refining it. Because the illumination condition was poor, the Basler took the photographs with an artificial gain that introduced some noise, which appeared as fine vertical highlight lines. Because the analysis is performed by pixel columns, we needed to smooth the image horizontally. The selected filter presents a constant known as lag ($n/2$, where n is the order). Each pixel needed to be moved $n/2$ to the left in order to restore the image. Figure 7 shows the graph of the pixel values of column 500 of the original photograph and the filtered data, which appears very smooth.



Figure 6. Frontal (left) and lateral (right) views.

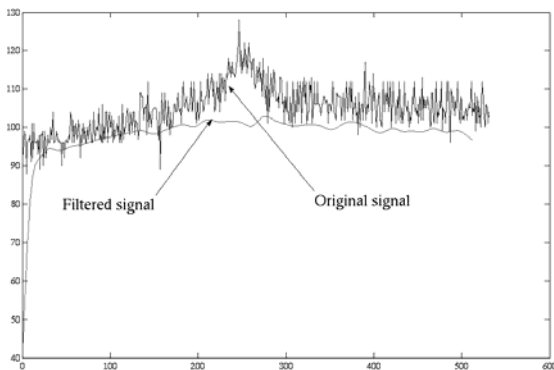


Figure 7. Filtered signal of column 500 of the image matrix.

Once the image had been filtered, we studied it, for example, by focusing on the pixels of column 460, shown in Figure 8. The maximum intensity (points with a high value) corresponds to the intersection between column 460 and the laser beams. The signal progressively descends from left to right. This implies that the bottom part of the photograph is a little darker than the upper part. The six maximum points representing the position of the lasers cannot be obtained because there may be other relative maximums that do not correspond to a laser beam. A more detailed algorithm was applied in order to detect the laser beams. A new FIR filter was also applied to the image in order to smooth the high-frequency noise signal. Figure 9 shows column 460 after being filtered and selected according to the lowest second derivative. Once the column had been filtered, practically the only peaks that remained were those that needed to be determined. A series of different pre-processing steps were carried out on the image before it was in the best condition for the beams and the surface to be surveyed. That is, some pixels not correctly detected in the image needed to be eliminated, some maximums were not real, etc. After this process, Figure 10 was obtained.

3.6 Laser-beam detection techniques. Lateral view.

Certain problems appeared in this situation. First, the resolution of the camera was lower (460x640) than that of the Basler, the lens was wide-angle and precision was lost because the density of information in the final image was lower. Second, the laser beams were seen in a tilted view and the detection of the maximum by columns was therefore discarded. A new technique, morphological image treatment, needed to be used in this image view (Serra, 1994).

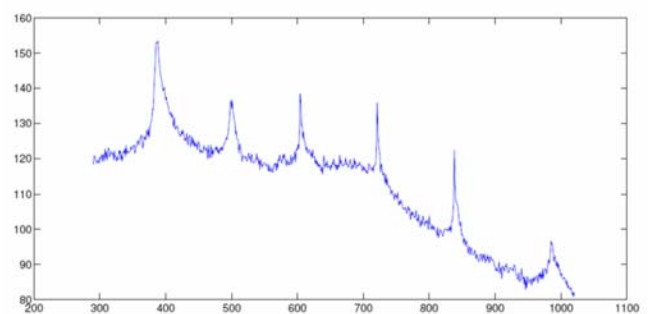


Figure 8. Pixel intensity distribution of column 460. The peaks are the laser beams.

The first step was to convert the image to a binary image by means of a threshold: 1 was given over a certain pixel threshold value and 0 was given to the rest. The threshold was chosen by reaching a compromise between losing good information and adding extra bad information. This made image treatment difficult, i.e. there were gaps in white areas, overlapping laser beams, etc. Figure 11 shows

the results obtained by applying different thresholds in the binary-conversion process.

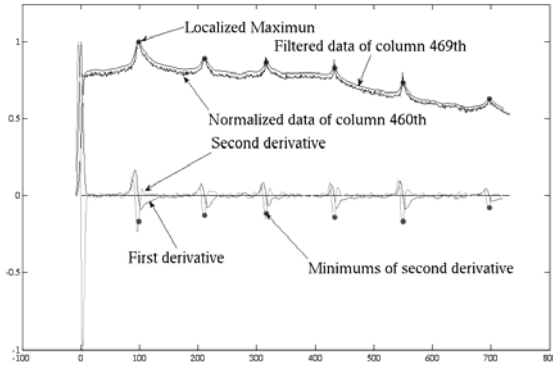


Figure 9. Column 460 filtered, localized and ordered by the lowest second derivative.

Once the image had been processed, the skeleton of the image was found. First, however, we made a series of corrections, as in the frontal view. We eliminated some spurious points and groups of points that interfered with the detection of the main laser beams. To do this, we used a MATLAB image function called “*bwmorph*” with options such as “Clean, Fill or Spur”. The image was then ready for the skeleton process.

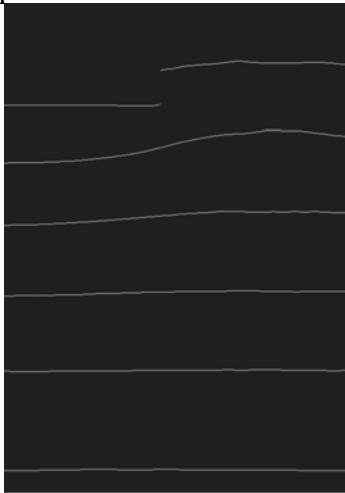


Figure 10. A frontal image taken by the Basler camera that has been treated mathematically.

We performed successive “*thinning*”, so the lines became thinner and thinner and the border pixels were erased until no change was noticeable. We used MATLAB and the image function with the “*thin inf*” option. Finally, dendrite forms grew indiscriminately from the main laser beams, and we generated a new code to trim the skeleton. Figure 12 shows different skeletons obtained with different procedures. Another procedure that worked well was applying a filter, before applying the threshold, defined by the matrix

$$h = \frac{1}{9} \begin{pmatrix} 0 & 0 & 1 & 1 & 1 \\ 0 & 1 & 1 & 1 & 0 \\ 1 & 1 & 1 & 0 & 0 \end{pmatrix} \quad (19)$$

which simply assigns the mean of the eight neighbours and itself and respects the laser direction.

Figure 12 shows that the application of this mean smooths the line and fills the gaps. The threshold is therefore necessary to obtain the skeleton.

4 RESULTS

We used frontal images taken with the Basler camera (Figure 10). The entire exercise involved 30 fps for 6 seconds.

Calibration: First, a vector x contains the calibration points in \mathbb{R}^3 and X represents its correspondents in the photograph. In this example, we added 195 calibration points from three different calibration box positions and some points on the floor in order to obtain the matrix projection

A column vector d was declared to contain the coordinates of the laser planes. The curve i belonging to the plane $x = d(i)$ was obtained.

Laser curve determination: If pixel value matrix A contains the photograph to be treated, the technique of maximum and the filter must be applied to smooth the image and to trim the dendrite forms attached to the main lines. Thus, we obtained a structure that had the proper pixel position and curve order.

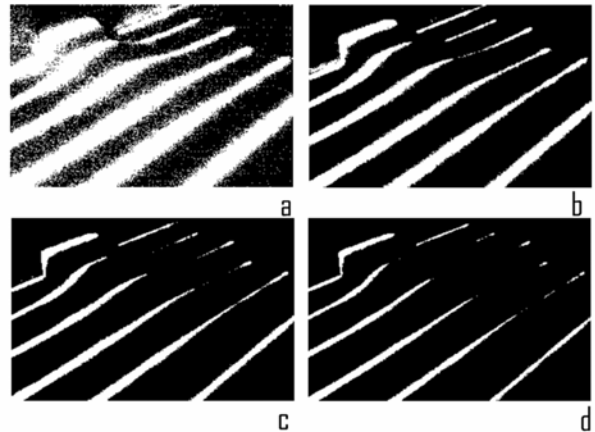


Figure 11. The process of applying different thresholds (a to d) caused a loss of information. The lines appear to be cut.

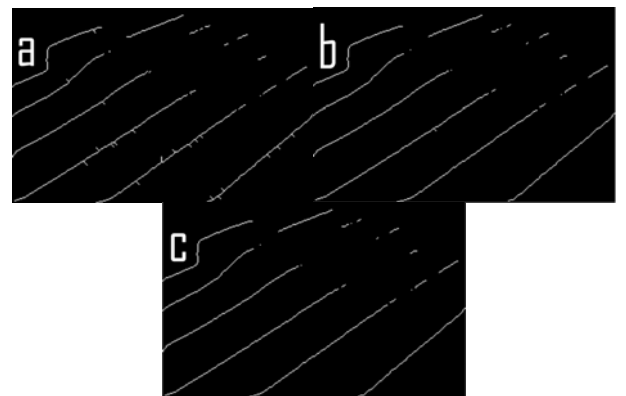


Figure 12. Results for different procedures. Dendrites are attached to the main lines.

Surveying: We then obtained the coordinates in \mathbb{R}^3 by applying the inverse transformation M , which

converts pixel coordinates into real coordinates. Figure 13 presents the results, which show how the water formed a vertical wall near the exit wall.

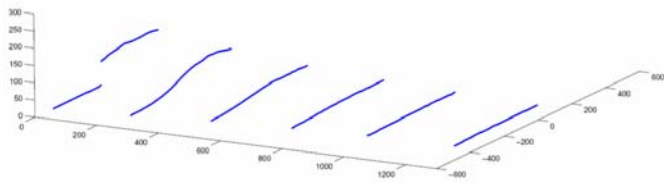


Figure 13 Reconstruction of laser beams from the Lumenera camera.

Results from the Basler camera position: Due to the excellent position and high-quality information of the Basler camera, a numerical/experimental comparison is presented here. The mixture of water and milk flowed very quickly across the platform, producing a jet flow that increased in width from 40 to 240 cm. The front of the flow moved very quickly, close to 342 cm/s, which was faster than the theoretical value of 221 cm/s given by the Ritter solution.

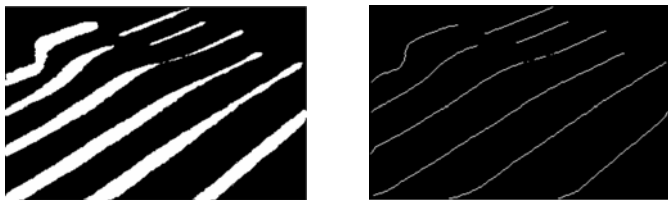


Figure 14. Result obtained by applying the mask given by the matrix of Equation (19).

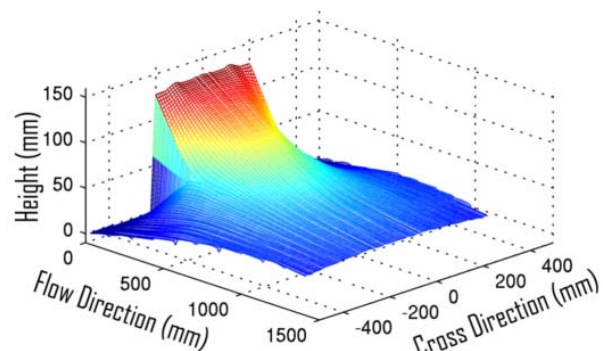


Figure 15. Experimental 3D surface from the Basler camera at 2.45 s.

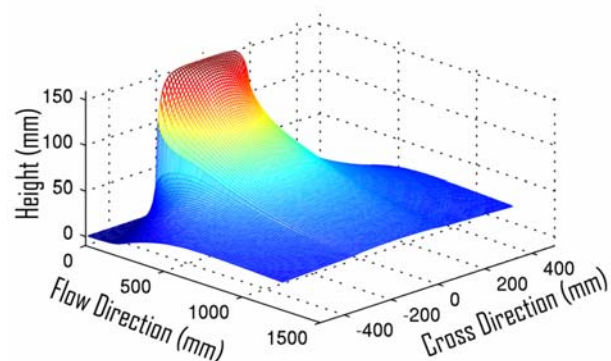


Figure 16. Numerical 3D water surface from FLATMODEL at 2.45 s.

Figure 15 and Figure 16 show the experimental and numerical results respectively. The numerical data were taken from FLATModel, which was created by GITS (some aspects are discussed in Medina et al. 2006), and the experimental data were obtained by interpolating Figure 13. The instant compared is 2.45 seconds after the flow passed the end of the flume. The numerical data has a smoother shape than the experimental data. Also, the flow of water is more vertical in the experimental images than in the numerical results. This is because reality is more complex than the 2D Saint-Venant solution. The vertical zones do not obey the Saint-Venant hypothesis. The shapes and heights appear similar in both representations but are slightly higher in the numerical results. The following comparison between experimental and numerical data refers to fan expansion. **¡Error! No se encuentra el origen de la referencia.** 17 shows all data below a height of 2 mm. The resulting angles are 36 and 23° for the numerical and experimental data respectively. The experimental fan opens faster than the numerical one.

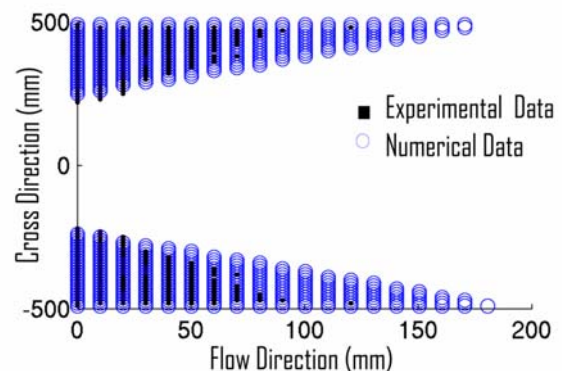


Figure 17. Comparison of the fan in the experimental and numerical data. $T = 2450$ ms. The data is cut off at a height of 2 mm.

Figure 18 and Figure 19 show the behaviour of the absolute error, which is calculated as the experimental data minus the numerical data. The numerical and experimental data agree throughout the area of study. The only regions that are very different are those which fail to meet the Saint-Venant conditions. Nevertheless, the comparison shows that the data that has an absolute error of less than 40% has a mean error of 13.9% throughout the area of study, whereas the data that has an absolute error of 20% has a mean error of 9%.

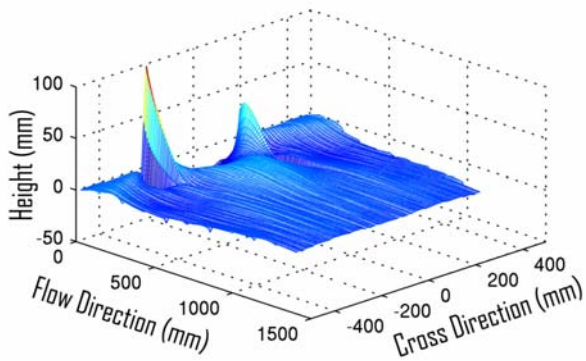


Figure 18. 3D diagram of absolute error. The highest errors are located in the area with high water gradients.

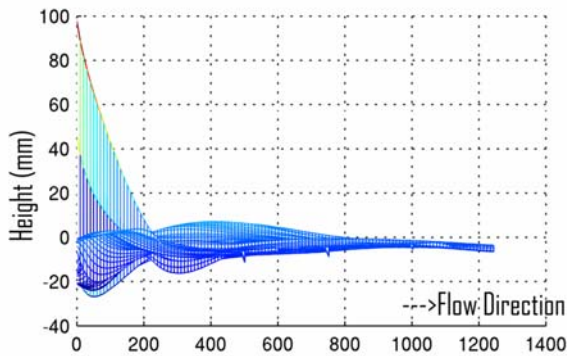


Figure 19. Lateral view of the absolute error surface data.

5 CONCLUSION

This paper presents a procedure that works well in 2D water-surface treatment. The camera must be properly calibrated and geometrical aberrations should be corrected if necessary. The use of Nikon or other high-quality lenses (and other pre-process corrections) clearly makes image processing easier. Milk is essential to obtaining clean, bright laser beams because only opaque liquids work well with laser light. The numerical/experimental comparison shows good agreement. The experimental data shows certain numerical difficulties in the high-gradient zone, where the Saint-Venant hypothesis fails due to the high curvature of the current lines and the non-hydrostatic pressure distribution. The overall absolute error for the surface showed good agreement, with a mean error of around 9% when the threshold is 20%.

6 ACKNOWLEDGMENTS

This study was funded by CICYT under project BTE2002-00375.

BIBLIOGRAPHY:

Abdel-Aziz, Y.I., & Karara, H.M. 1971. Direct linear transformation from comparator coordinates into object

space coordinates in close-range photogrammetry. Proceedings of the Symposium on Close-Range Photogrammetry (pp. 1-18). Falls Church, VA: American Society of Photogrammetry.

Chen L, Armstrong CW, Raftopoulos DD. 1994. An investigation on the accuracy of three-dimensional space reconstruction using the direct linear transformation technique. *J Biomech.*;27(4):493-500.

Faugeras, O. 1993. *Three-Dimensional Computer Vision: A Geometric Point of View*. MIT Press.

González, Rafael and Woods, Richard (1992). *Digital Image Processing*. Addison Wesley Publishing Company, Inc.

Hatze H. 1988 High-precision three-dimensional photogrammetric calibration and object space reconstruction using a modified DLT-approach. *J. Biomech.*; 21(7):533-8.

Hecht, Eugene 2000. *Optics*. Addison Wesley.

Kofman, J., Miller, D. L., Knopf, G. K., Zecevic, A. 1998. Calibration and measurement accuracy of a stereophotogrammetric system using the direct linear transformation. North American Congress on Biomechanics. University of Waterloo/Waterloo, Ontario, Canada

Medina, V., Bateman, A. and Velasco, D. A New Approach to Solve the Boundary Conditions in the Shallow Water Equations Using a Riemann Solver. *River Flow 2006*, Lisbon, Portugal.

Olague, G. and Ramírez, R. 2001. Artificial Image Generation from Digital Images. American Society of Photogrammetry and Remote Sensing (ASPRS).

Pizarro, Campos and Tozzi 2005. Comparación de técnicas de calibración de cámaras digitales. *Rev. Fac. Ing.-Univ. Tarapacá*. Vol. 13.

Pribanic, T.; Sturm, P. Cifrek, M. 2005. Proceedings of the 4th International Symposium on Image and Signal Processing and Analysis, 2005. ISPA 2005. ISSN: 1845-5921

Sánchez Moreno, Francisco 2000. *Reconstrucción 3D con iluminación láser: aplicaciones a la fotogrametría industrial*. UPM-DISAM r T-2000.31v1.0

Serra, J. and Soille, P. eds., 1994: *Mathematical Morphology and its Applications to Image Processing*, Kluwer Academic Publishers, Dordrecht-Boston-London.